Int. J. Heat Mass Transfer. Vol. 31, No. 3, pp. 525–539, 1988
Printed in Great Britain

0017–9310/88 $3.00 + 0.00
Pergamon Press plc

The stability chart of parallel shear flows with double diffusive processes—approximate derivation by a first-order Galerkin method

M. MAGEN,† D. PNUELI and Y. ZVIRIN
Faculty of Mechanical Engineering, Technion, Israel Institute of Technology, Haifa 32000, Israel

(*Received* 18 *November* 1986 *and in revised form* 26 *June* 1987)

Abstract—The stability of an infinite fluid layer subject to arbitrary horizontal shear flow and to arbitrary vertical temperature and salinity distributions is considered. Linear stability analysis is used to investigate the stability under general three-dimensional (3-D) perturbations. A first approximation Galerkin method is used to derive the characteristic equation; then conditions for stability are obtained and the marginal stability lines can be found. The method is applied in an example with a parabolic velocity distribution and linear temperature and salinity profiles. The stability chart in the plane of the Rayleigh numbers is found to include various stable and unstable regions, depending on the Reynolds number. The results obtained here are compared with previous results derived by a general Galerkin method. A region is found where the flow in stable for two-dimensional (2-D) transverse perturbations but unstable with respect to general 3-D disturbances.

1. INTRODUCTION

THE STABILITY of double diffusive flows has important implications in geophysical phenomena and engineering applications, including energy conversion systems, and in particular the solar pond.

The stability of a stagnant fluid layer with a vertical temperature distribution but not salinity effects has been studied by numerous investigators, cf. the surveys by Ostrach [1] and Chandrasekhar [2].

In most of the studies of thermal stability the 'conventional' Boussinesq approximation is adopted, i.e. the density is considered constant in the governing equations except for the body force term in the momentum equation. This term is represented by assuming a linear relation between the density and temperature. There are many cases where this assumption is not justified; Qureshi and Gebhart [3] recently considered such a case and showed the effect of the realistic density changes.

In treating problems of thermal or double diffusive stability, the steady-state solution is usually assumed to be known, and its stability is investigated using linear or non-linear approaches. The linear stability analysis leads, generally, to an eigenvalue problem, which can be expressed in a simple form, at least when the temperature gradient is constant. The principle of exchange of stabilities holds in this case, and instability develops in a monotonic fashion at a critical Rayleigh number. Veronis [4] showed that for double diffusive processes (with temperature and salinity gradients) this principle is not always valid and the onset of instabilities can be associated with oscillations. Exact conditions for oscillatory instability were given by Pnueli and Iscovici [5]. The eigenvalue problem in this case has an operator which is not self-adjoint. Moreover, the operator in the Orr–Sommerfeld equation, which governs instabilities in horizontal shear flows, is also not self-adjoint, e.g. Orszag [6].

The present work considers all three effects: temperature gradients, salinity variations and horizontal shear flows. Magen *et al.* [7] summarized the relevant literature dealing with double diffusive stability and the influence of Reynolds number on the stability boundary. They presented a detailed discussion of the properties of the stability chart for double diffusive flows, using the governing equations only, but not their solutions for any particular case. The operator in the corresponding eigenvalue problem is evidently not self-adjoint, thus ruling out some more conventional methods of solution, e.g. methods utilizing extremum properties of the eigenvalues for self-adjoint operators.

Magen *et al.* [8] applied the general method of ref. [7] to derive the stability chart of double diffusive shear flows in the Rayleigh numbers plane, using a numerical technique based on general Galerkin and continuation methods.

The main disadvantage of the Galerkin method is the high order of approximations usually required, e.g. ref. [6]. On the other hand, Nield [9] pointed out that the first-order approximation sometimes provides very good results. The results obtained in ref. [8] are accurate, but require significant computer time and memory, because they involve calculations of eigenvalues of complex high order matrices, see also refs. [6, 10]. Moreover, when the order, i, of the Galerkin method is increased to achieve convergence and

† Present address: Department of Applied Mathematics, The Weitzman Institute of Science, Rehovot, Israel.

NOMENCLATURE

A_j coefficients, equations (A3)
a_k coefficients of characteristic equation (8), b_k+ic_k
B_k coefficients, equations (A3)
$B_d, B_{rest}, B_R, B_{Re}$ stability boundaries: dynamic, static, for R and for Re, respectively
D_k coefficients, equations (A3)
D d/dz
E_K coefficients, equations (15)
h_{u_j}, h_{l_j} Biot numbers, equations (4)
$\hat{i}, \hat{j}, \hat{k}$ unit vectors
L_K stability condition parameters, equations (9)
L_{K0} stability condition parameters, equations (12)
l_3 stability condition parameter, equations (15)
l_{20}, l_{40} axes in the abstract l_{20}–l_{40} plane, equations (15)
M_{ij}, N_{ij} elements of 3×3 matrices M, N, equation (7)
p pressure
P_1, P_2 Prandtl and Schmidt numbers, respectively
Re Reynolds number
R $\beta_x Re$
r parameter, equations (15)
S_1, S_2 Rayleigh numbers for temperature and salinity
T_1, T_2 temperature and salinity fields
$\mathring{T}_1, \mathring{T}_2$ undisturbed temperature and salinity
T_{ji} complex coefficients, equations (6)
t time
$\mathring{u}$ undisturbed horizontal velocity
$\hat{u}_i, \hat{v}_j, \hat{w}_i$ three components of the velocity field
x, y, z Cartesian coordinates, x in the flow direction and z in the vertical direction.

Greek symbols
β_x, β_y horizontal wave numbers
β^2 $\beta_x^2+\beta_y^2$
δ_i, ξ_{ij} parameters, equations (12)
η, γ, γ_0 parameters dependent on β, equations (A9)
ρ density
σ stability parameter, equation (2)
ϕ, θ_j trial functions, equations (6).

Superscripts
$(\tilde{x})$ disturbed state
$(\mathring{x})$ undisturbed state
$(x)^*$ critical stability parameter.

Special symbol
$\langle\ldots\rangle$ $\int_0^1 \ldots dz$.

better accuracy, a new eigenvalue problem must be solved for every i and the results of the previous calculations (lower i) cannot be used. Therefore, a simpler method for the stability study would be advantageous, even at the cost of accuracy reduction.

The present work uses a first-order Galerkin method to obtain an approximation for the stability chart and compares it with more accurate calculations. The basic conservation equations and linear stability analysis lead to the characteristic equation for the stability parameter in the form of a third-order polynomial with complex coefficients. A new derivation is presented for the stability conditions of such an equation.

The stability chart is first obtained for two-dimensional (2-D) perturbations in the flow direction. The Squire transform [11] is used, together with the general results of ref. [7], in order to find the stability chart for arbitrary three-dimensional (3-D) disturbances. The properties of the chart in an abstract plane of the parameters are discussed for the most general case. Examples are given for the behaviour of the stability boundary for special cases in the plane of the Rayleigh numbers.

The setting of the eigenproblem and the choice of the trial functions is more different in this work than those of ref. [8]. The results show quite good agreement with the accurate stability boundary obtained by ref. [8] and with other known results for simple cases. Furthermore, an unstable region is found here in the parametric space, where the flow is stable for 2-D disturbances. This result was predicted in the general analysis of ref. [7], but could not be verified by the high order Galerkin method of ref. [8] due to convergence problems. Magen and Patera [12] have recently shown, for the simpler case of a plane Poiseuille flow, that there may exist oblique unstable disturbances while both perturbations in the flow direction (transverse rolls) and perpendicular to it (longitudinal rolls) are stable.

It is finally noted that the first-order formulation developed here cannot be extended systematically to higher orders. Section 6 includes a detailed discussion of the applicability and accuracy of the method.

2. DERIVATION OF THE CHARACTERISTIC STABILITY EQUATION AND THE STABILITY CRITERIA

Reference [7] includes a derivation of the governing equations for small perturbations superimposed on an undisturbed double diffusive steady flow state. The

velocity, pressure, density, temperature and salinity fields ($\tilde{\mathbf{V}}, \tilde{p}, \tilde{\rho}, \tilde{T}_1, \tilde{T}_2$) are expressed as

$$\tilde{\mathbf{V}} = \mathring{\mathbf{V}} + \mathbf{V} = \mathring{u}(z)\hat{i} + (u\hat{i} + v\hat{j} + w\hat{k});$$
$$\tilde{p} = \mathring{p} + p; \quad \tilde{\rho} = \mathring{\rho} + \rho; \quad \tilde{T}_j = \mathring{T}_j(z) + T_j; \quad j = 1,2 \tag{1}$$

where the undisturbed distributions are denoted by (°). Horizontal flows are considered, with the coordinate x in the flow direction and the steady state distributions $\mathring{u}$ and $\mathring{T}_j$ are assumed to depend on the vertical coordinate, z, only. The perturbations, taken to be small, are expressed in the form

$$\{\mathbf{V}(x,y,z,t); T_j(x,y,z,t); p(x,y,z,t)\} = \{\mathbf{V}(z); T_j(z); p(z)\} \exp[\mathrm{i}(\beta_x x + \beta_y y) + \sigma t]; \quad j = 1,2 \tag{2}$$

where σ is the stability parameter and β_x and β_y are horizontal wave numbers in the flow direction and perpendicular to it.

The variables in equations (1) and (2) are introduced into the continuity, momentum, energy and diffusion equations and use is made of the equation of state in the form of a linear relation between the density and the temperature and salinity. The Boussinesq approximation is adopted and a linear stability analysis is performed, whereby second-order terms are neglected in the governing equations. The pressure terms are eliminated and the variables are normalized in a standard way (see equation (8) in ref. [7] and also ref. [8]), leading to the dimensionless perturbation equations

$$\left.\begin{aligned} &(\mathrm{D}^2 - \beta^2 - \mathrm{i}RP_j\mathring{u})T_j + \mathrm{D}\mathring{T}_j w = \sigma P_j T_j; \quad j = 1,2 \\ &-\{(\mathrm{D}^2-\beta^2)^2 - \mathrm{i}R[\mathring{u}(\mathrm{D}^2-\beta^2) - \mathrm{D}^2\mathring{u}]w \\ &\qquad + \beta^2(S_1T_1 - S_2T_2) = -\sigma(\mathrm{D}^2-\beta^2)w \end{aligned}\right\} \tag{3}$$

where $\mathrm{D} \equiv \mathrm{d}/\mathrm{d}z$, $\beta^2 \equiv \beta_x^2 + \beta_y^2$, $R \equiv \beta_x\, Re$, Re is the Reynolds number, based on the volumetric flow rate

$$Q = \int_0^d \mathring{u}\,\mathrm{d}x$$

(here $\mathring{u}(z)$ is the dimensional velocity); $P_{1,2}$ are the Prandtl and Schmidt numbers and $S_{1,2}$ are the Rayleigh numbers for temperature and salinity: $P_j \equiv \nu/K_j$; $S_j = g\Delta T_j \alpha_j d^3/\nu K_j$. Here ν is the kinematic viscosity, K_j the thermal and concentration diffusivities, g the acceleration of gravity, ΔT_j the characteristic temperature and salinity differences, α_j are the respective expansion coefficients and d is a characteristic length (the depth of the layer).

It is noted that the symbols used here for the concentration field, the Schmidt number and the Rayleigh numbers differ from those used conventionally. The main reason for it is convenience of presenting the equations and results in a more compact manner.

The boundary conditions are given by

$$\left.\begin{aligned} &w = 0;\ \mathrm{D}^2 w = 0 && \text{free boundary} \\ &w = 0;\ \mathrm{D}w = 0 && \text{solid boundary} \\ &\mathrm{D}T_j + h_{u_j}T_j = 0 && \text{upper boundary}, j = 1,2 \\ &-\mathrm{D}T_j + h_{l_j}T_j = 0 && \text{lower boundary}, j = 1,2 \end{aligned}\right\} \tag{4}$$

where h_{u_j} and h_{l_j} are Biot numbers for temperature and salinity (or dimensionless heat and mass transfer coefficients).

Equations (3) and (4) constitute the mathematical definition of the stability problem; it is an eigenvalue problem, set by three ordinary differential equations with complex coefficients. This problem is not self-adjoint and the stability parameter σ cannot be assumed real. The stability criteria, for the eigenvalue with the largest real part, are

$$\mathrm{Re}(\sigma) < 0 \quad \text{stability};$$
$$\mathrm{Re}(\sigma) = 0 \quad \text{marginal stability}. \tag{5}$$

For given $\mathring{u}(z)$, $\mathring{T}_1(z)$, $\mathring{T}_2(z)$, the flow is stable when the combination of the physical parameters of the problem $\{h_{u_j}, h_{l_j}, P_j, S_j, Re\}$ guarantees that condition (5) is satisfied for every mode (i.e. for every wave number β and β_x in the range $0 \leqslant \beta < \infty$, $0 \leqslant \beta_x \leqslant \beta$).

A first approximation Galerkin method is used here to derive the characteristic stability equation from the perturbation equations (3). Let the eigenfunctions be expanded in a series of a complete sequence of trial functions that satisfy the boundary conditions. Now restrict the treatment to the first elements of the series, i.e.

$$w = w_1\phi(z); \quad T_j = T_{j1}\theta_j(z) \tag{6}$$

where w_1, T_{j1} are complex constants and the functions $\phi(z)$, $\theta(z)_j$ satisfy boundary conditions (4).

The Galerkin method, cf. Mikhlin [13], consists of the substitution of equations (6) into equations (3) and the requirement that the first of equations (3) be orthogonal to $\theta_1(z)$, the second one be orthogonal to $\theta_2(z)$ and the third be orthogonal to $\phi(z)$. These operations result in

$$[N]\begin{Bmatrix} T_{11} \\ T_{21} \\ w_1 \end{Bmatrix} = \sigma[M]\begin{Bmatrix} T_{11} \\ T_{21} \\ w_1 \end{Bmatrix} \Rightarrow |N - \sigma M| = 0 \tag{7}$$

where the elements of the (3×3) matrices N and M are defined in the Appendix. Equation (7) is the characteristic equation for σ. It is an algebraic equation of the third order with complex coefficients, which can be written as

$$\sigma^3 + a_1\sigma^2 + a_2\sigma + a_3 = 0 \tag{8}$$

where the coefficients a_j are also listed in the Appendix. Stability conditions (5) require that the three roots of the characteristic equation (8) have

negative or zero real parts. These conditions lead to the following relations:†

$$L_1 > 0, L_2 > 0, L_3 > 0 \quad \text{definite stability} \quad (9a)$$

$$\left.\begin{array}{ll} L_1 > 0, L_2 > 0, L_3 = 0 & \text{marginal} \\ L_1 > 0, L_2 = L_3 = 0, L_4 \geqslant 0 & \text{stability lines} \end{array}\right\} \quad (9b), (9c)$$

$$L_1 = L_2 = L_3 = 0 \quad \text{additional conditions (see below)} \quad (9d)$$

where (see also the Appendix)

$$L_1 = b_1;\ L_2 = c_2(c_1b_1 - c_2) + b_1^2b_2 - b_1b_3;$$
$$L_3 = L_2^2L_4 - (L_2c_2 + 2b_1L_5)^2 \quad (10)$$
$$L_4 = c_2^2 + 4b_1b_3;\ L_5 = b_3(c_1b_1 - c_2) - b_1^2c_3$$
$$b_k = \mathrm{Re}\,(a_k);\ c_k = \mathrm{Im}\,(a_k);\ k = 1, 2, 3.$$

It is noted that in case (9a) for definite stability all three roots of equation (8) have negative real parts. In case (9b) the equation has one root with $\mathrm{Re}\,(\sigma) = 0$, $\mathrm{Im}\,(\sigma) = L_5/L_2$ and the two other roots have negative parts. In case (9c) the characteristic equation has two roots with zero real parts and imaginary parts given by $(-c_2 \pm \sqrt{L_4})/2L_1$ and the negative real part equal to $-L_1$. In this case the additional condition $L_4 \geqslant 0$ has to be used, which is identically satisfied in cases (9a) and (9b), see equations (10) for L_3. Finally, in case (9d) all three roots have no real part.

At this stage it is possible to extract some intermediate results.

(1) The first condition in equations (9a)–(9c), namely $L_1 > 0$, is identically satisfied as can be seen from equations (10) and (A1)–(A5). It also follows that case (9d) is irrelevant because L_1 is always positive. This means that condition (9) reduces to

$$L_2 > 0,\ L_3 > 0\ (L_4 \geqslant 0) \quad \text{definite stability} \quad (11a)$$

$$\left.\begin{array}{ll} L_2 > 0,\ L_3 = 0\ (L_4 \geqslant 0) & \text{marginal} \\ L_2 = L_3 = 0,\ L_4 \geqslant 0 & \text{stability lines.} \end{array}\right\} \quad (11b), (11c)$$

(2) Parameters L_2, L_4 and L_5 are linear functions of Rayleigh numbers S_1 and S_2, see equations (A5), (A3) and (A1).

(3) As observed from equations (A5), L_2, L_3 and L_4 depend on R^2 and therefore on Re^2. This means that the stability conditions also depend on Re^2.

(4) The multipliers of R^2 in equations (A5) for L_2 and L_4 are non-negative (details are given by Magen [15]). The importance of this observation is clarified below.

Finally, L_2, L_3 and L_4 can be found from equations (A1), (A3) and (A5). Introduction of the results into equations (11) yields the stability conditions for every special case.

† A complete procedure of obtaining equations (9), which are a generalization of the Routh–Hurwitz conditions for a complex polynomial, appear in Gantamakher [14]. Equivalent conditions have been derived in a simpler form by Magen [15] for the third degree polynomial considered here.

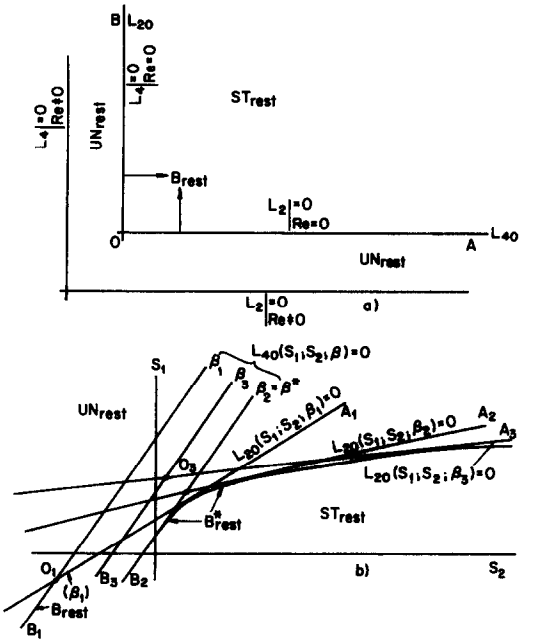

FIG. 1. Static marginal stability boundaries: (a) in the L_{40}–L_{20} plane; (b) in the Rayleigh number plane, S_1–S_2.

3. MARGINAL STABILITY LINES AND STABILITY REGIONS

3.1. *Static stability*

For the case of no initial flow, $Re = R = 0$, it is found from equations (10), (A4) and (A5) that the relevant parameters L reduce to

$$\left.\begin{array}{l} L_2|_{R=0} \equiv L_{20} = \delta_2(\beta) - \xi_{21}(\beta)S_1 + \xi_{22}(\beta)S_2 \\ L_4|_{R=0} \equiv L_{40} = \delta_4(\beta) - \xi_{41}(\beta)S_1 + \xi_{42}(\beta)S_2 \\ L_{30} = L_{20}^2L_{40};\quad L_{50} = 0 \end{array}\right\} \quad (12)$$

where coefficients δ_j and ξ_{j1} defined in equations (A6) depend only on wave number β. Stability criteria (11) can now be written as

$$L_{20} > 0,\ L_{40} > 0 \quad \text{definite stability} \quad (13a)$$

$$\left.\begin{array}{ll} L_{20} > 0,\ L_{40} = 0 & \text{marginal} \\ L_{20} = 0,\ L_{40} \geqslant 0 & \text{stability lines.} \end{array}\right\} \quad (13b), (13c)$$

This means that in the plane L_{20}–L_{40} the static stability domain is the first quadrant and we denote it by ST_{rest}. The static instability domain (the three other quadrants) are denoted by UN_{rest}. The boundary between them (positive parts of the axes L_{20}, L_{40}) is denoted B_{rest}, see Fig. 1(a).

The marginal stability boundary B_{rest} is now transformed to the Rayleigh number plane. The relations between S_1–S_2 and L_{20}–L_{40} are linear and they include the wave number, β, cf. equations (12) and (A6). Thus, for a *specific* β, B_{rest} in the plane S_1–S_2 is also formed by the intersection of the two straight lines, $L_{20} = 0$

and $L_{40} = 0$, see Fig. 1(b). However, the stability condition for *any* β is sought. Therefore, we seek the envelope of the family of lines $B_{\text{rest}}(S_1, S_2, \beta)$ depending on the parameter β, i.e.

$$\left.\begin{aligned} \xi_{k_1}(\beta)S_1 - \xi_{k_2}(\beta)S_2 &= \delta_k(\beta) \\ \xi'_{k_1}(\beta)S_1 - \xi'_{k_2}(\beta)S_2 &= \delta'_k(\beta) \end{aligned}\right\} k = 2,4 \qquad \begin{aligned} &(14a) \\ &(14b) \end{aligned}$$

where the prime denotes differentiation with respect to β. The wave number β can be eliminated between equations (14) and the static stability boundary B^*_{rest} is thus obtained as the envelope, shown qualitatively in Fig. 1(b).

3.2. *Dynamic stability*

The dynamic stability boundary for cases with initial flows ($Re \neq 0$), is determined from equations (11). This marginal stability curve ($L_3 = 0$, $L_2 \geqslant 0$, $L_4 \geqslant 0$) depends on both wave numbers β and β_x for any specific value of Re ($R = Re\,\beta_x$). We are interested, however, in the general stability margins, which are independent of β and β_x, i.e. the stability boundary for any arbitrary perturbation. The Squire transformation will now be used, whereby only 2-D disturbances in the flow direction ($\beta_x = \beta$) are considered. The marginal stability line, B_{2d}, will first be constructed for this case and for a specific wave number β: $R = \beta\, Re$. Then the results of ref. [7] will be applied to derive the line B_{3d} for general 3-D perturbations.

According to ref. [7], the general stability chart for any Re includes 'true' segments of the marginal stability curves for 2-D perturbations, where these are the most unstable. The 'dummy' parts of the curves (where 2-D disturbances are stable but 3-D need not be stable) are excluded and replaced by the envelope of these lines and by parts of the static stability lines.

The line B_{2d} is determined from equation (11b) as $L_3 = 0$ for a specific value of R. Additional conditions are also imposed, namely $L_2 \geqslant 0$ and $L_4 \geqslant 0$. It can be shown that the coefficients of Re^2 in the expressions for L_2 and L_4, equations (A5), are non-negative. Therefore, an increase of Re will cause movement of the boundary lines $L_2 = 0$, $L_4 = 0$ into the region UN_{rest} in the plane L_{20}–L_{40}, see Fig. 1(a). It seems as if this result indicates an increase of the stability domain, determined by the lines $L_3 = 0$, $L_2 = 0$ and $L_4 = 0$. According to ref. [7], however, an increase of Re cannot stabilize unstable states, thus the lines $L_2 = 0$, $L_4 = 0$ ($Re \neq 0$) are 'dummy parts'. Therefore, instead of inequalities $L_2 > 0$, $L_4 > 0$ one should use $L_{20} > 0$, $L_{40} > 0$, and only these parts of the line B_{2d} which belong to the first quadrant of the plane L_{20}–L_{40} should be considered.

The transition from B_{2d} to B_{3d} and the transformation to the physical plane S_1–S_2 are now discussed for the special case of identical boundary conditions for temperature and salinity.

4. THE STABILITY CHART FOR THE CASE OF IDENTICAL BOUNDARY CONDITIONS FOR TEMPERATURE AND SALINITY

Consider the special case where the boundary conditions for the temperature and the salt concentration in equations (4) are identical. There is no restriction, however, on the initial distributions $\hat{T}_1(z)$, $\hat{T}_2(z)$, which need not be the same. We choose for this case identical trial functions for the temperature and salinity perturbations: $\theta_1(z) = \theta_2(z) = \theta(z)$.

In order to simplify the treatment of the equations, the parameters L_{20}, L_{40}, L_3 and R are transformed using the relations

$$\left.\begin{aligned} L_{20} &= l_{20}E_2(\beta); \quad L_{40} = l_{40}E_4(\beta) \\ L_3 &= l_3 E_3(\beta); \quad R^2 = r^2 E_r(\beta) \end{aligned}\right\} \qquad (15)$$

$$l_3 = (l_{20}+2r^2)^2(l_{40}+r^2) - r^2(l_{20}+l_{40}-1+2r^2)^2 \qquad (16)$$

where coefficients $E(\beta)$, defined in equations (A8), are all positive, and equation (16) has been obtained by introduction of equations (15) into equations (10) for L_3.

The result of the derivation in the previous section was that the dynamic marginal stability line, B_{2d}, is determined by the conditions $l_3 = 0$, $l_{20} \geqslant 0$, $l_{40} \geqslant 0$. The expression for l_3, equation (16), does not include the physical parameters of the system. Therefore, it is more convenient to first construct the general stability chart in the l_{20}–l_{40} plane, which is the same for all the different cases, and only then to transform it to the Rayleigh number plane S_1–S_2, using equations (12) and (15).

Section 4.1 and Figs. 2 and 3 include a detailed derivation of the stability chart in the former plane and a discussion of its properties. The marginal stability lines, B_{2d}, are first constructed for various values of R (or r). Then the envelope, B_d, of the family of these lines is found (the line B_d is the stability boundary for all values of Re). Finally, margins B_{3d} are obtained, which determine the stability for specific values of Re.

4.1. *Construction of the stability boundary in the abstract plane* l_{20}–l_{40}

The marginal stability line $B_{2d}(l_3 = 0)$ for a specific wave number β, is obtained in the plane l_{20}–l_{40} from equation (16) as

$$l_{20} = \pm r[\sqrt{(l_{40}+r^2)} \mp r - 1/(\sqrt{(l_{40}+r^2)} \mp r)]. \qquad (17)$$

As indicated in the previous sections, the static stability region, ST_{rest}, is the first quadrant in the plane l_{20}–l_{40} (or L_{20}–L_{40}). Stable flows cannot correspond to points outside of this quadrant and those parts of B_{2d}, equation (17), not belonging to it are 'dummy' parts.

Different marginal stability curves correspond to

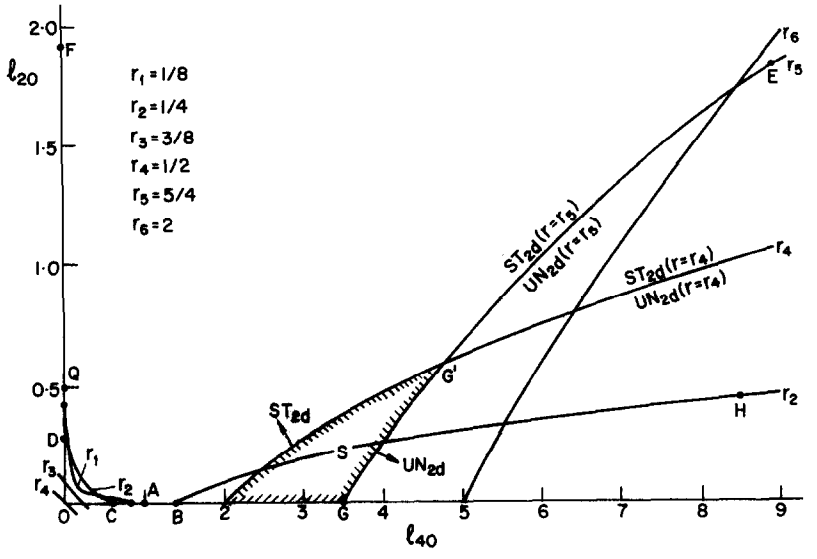

FIG. 2. Dynamic marginal stability boundaries B_{2d} for various values of r (or R) in the l_{40}–l_{20} plane.

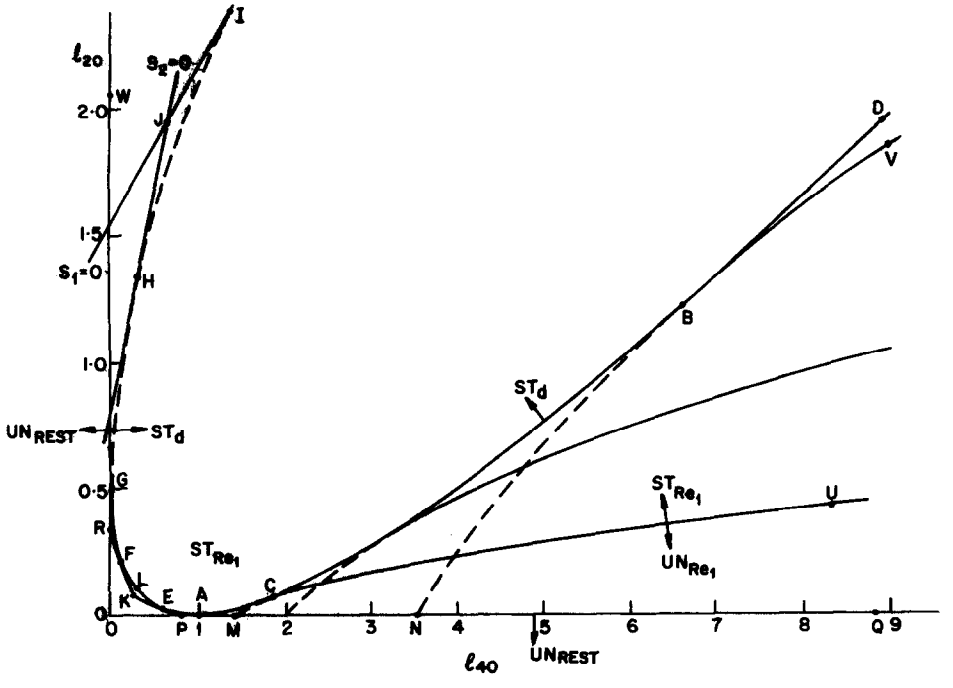

FIG. 3. Dynamic marginal stability boundaries B_{Re} for various Reynolds numbers and their envelope B_d in the l_{40}–l_{20} plane.

different values of r, defined in equations (15), as shown in Fig. 2. When $r < 1/2$ the boundary B_{2d} contains two branches of the line $l_3 = 0$ (equation (17)), e.g. DC and BH for $r = r_2$. As $r \to 0$ the right-hand branch of line (17) approaches the positive l_{40} axis from point A in Fig. 2, while the left-hand branch tends to merge with the broken line QOA on both axes; thus the static stability boundary is reconstructed for $r = 0$ (and $R = 0$).

In the limiting case $r = 1/2$, the left-hand branch of equation (17) passes through the origin and does not contribute to the stability boundary, which consists of the positive l_{20} axis, the part $0 \leqslant l_{40} \leqslant 2$ on the l_{40} axis and the right-branch of equation (17) (for $r = r_4 = 1/2$), see Fig. 2.

When $r > 1/2$ line B_{2d} has only one branch in the first quadrant, e.g. GE for $r = r_5$ in Fig. 2.

The stability region for a specific value of $r \sim Re$ lies above the line B_{2d} for this r. Now consider the region S in Fig. 2. The mathematical treatment for

2-D disturbances yields the conclusion that this region is stable for r_5 and unstable for r_4, with $r_4 < r_5$. According to the general results of ref. [7] (see also ref. [12]), any point in this region is unstable for r_5 with respect to general 3-D perturbations but stable for 2-D disturbances both in the flow direction (transverse rolls) and perpendicular to it (longitudinal rolls). It then follows that part GG′ of B_{2d} (for $r = r_5$) is a 'dummy' part. In order to separate the 'dummy' and 'true' parts of B_{2d}, and to derive the stability margin B_{3d} for a specific Reynolds number and 3-D disturbances, we proceed by constructing the envelope, B_d, of the family of lines B_{2d} with r as a parameter. It is obtained from equations (16) and (17) by the formal requirements

$$l_3(l_{20}, l_{40}, r) = 0; \quad \frac{dl_3}{dr} = 0 \tag{18}$$

leading to the envelope equation, B_d

$$l_{20} = (\sqrt{l_{40}} \pm 1)^2/2 \quad \text{envelope}, B_d. \tag{19}$$

The value of r on the envelope is given by

$$r^2 = \mp l_{20}\sqrt{l_{40}}/2 = \mp\sqrt{l_{40}}(\sqrt{l_{40}} \pm 1)^2/4. \tag{20}$$

The marginal stability curve B_d, equation (19) is a parabola in the plane l_{20}–l_{40}, e.g. the line **DBCAGI** in Fig. 3. Branch IHG is meaningless because r^2 on it is negative (see equation (20)). Therefore, the continuation of the marginal stability curve is the positive l_{20} axis, i.e. GW. The region above the line B_d is stable for any value of Re and for any general 3-D disturbance and is denoted ST_d.

It can be seen from equation (20) that the parameter r has a maximum on the envelope (point L in Fig. 3)

$$\frac{dr^2}{dl_{40}} = 0 \Rightarrow r_c = 1/27. \tag{21}$$

As we move along the line B_d, from point D to point A, r decreases to zero; then from A to L r increases to the value r_c and from L to G r decreases, again, to zero. As mentioned above, r^2 becomes negative as we continue to move along B_d towards points H and I.

For a value of r lower than r_c, say r_1, the marginal stability line B_{2d} has two branches RFKEP and MCU, touching the envelope B_d at three points F, E and C. When $r > r_c$ the line B_{2d} is tangent to B_d at a single point, e.g. point B of branch NBV for r_5.

From the stability chart in Fig. 3 and from the results of ref. [7] it can be seen that the segments of the lines B_{2d} lying between the envelope, B_d, and the axes l_{20}, l_{40} are 'dummy' parts, e.g. parts RF, EP and MC for $r = r_1$, and NB for $r = r_5$. It is interesting to follow now a complete path of a marginal stability line, B_{3d}, for a specific value of Re, say Re_1, which corresponds to r_1 (Fig. 3). According to the construction procedure already described, the line consists, first, of the 'true' parts of the stability boundary, B_{2d}, for 2-D perturbations, i.e. segments where these are the most dangerous, or easiest to excite. The line B_{3d} continues on the envelope or the l_{20} axis from the point where the line B_{3d} (for Re_1) is tangent to these lines.

Thus B_{3d} (Fig. 3) includes the 'true' part UC, then the segment CAE on the envelope B_d, the 'true' segment EKF, another part $-$FG, of the envelope, and, finally, the segment GW on the l_{20} axis, which is a part of the static stability line.

The results of this section based on the general results of ref. [7], can be summarized now for the stability chart for general 3-D perturbations.

The whole plane l_{20}–l_{40} is divided into four different parts for any specific wave number β (Fig. 3).

(1) Unstable region UN_{rest}: the whole plane except for the first quadrant. In this region all points are unstable for all values of Re.

(2) Stable region ST_d: above the line B_d; in this region all points are stable for all values of Re.

(3) Dynamic stability region ST_{Re} for $r \sim Re$: this region is the domain between lines CD and CU and the area FKELF, when it exists (i.e. for $r_1 < r_c$). In this region all points are stable for $Re < Re_1$.

(4) Dynamic unstable region ST_{Re_1} for $r \sim Re$: the area QACU and the part AOGFKEA for $r_1 < r_c$ (or the whole area GAO, for $r_1 > r_c$). In this region all points are unstable for $Re > Re_1$.

This concludes the derivation of the stability chart in the abstract l_{20}–l_{40} plane and the discussion of its properties. As mentioned above, the chart for a specific value of wave number β, is general and does not depend on the physical parameters of the problem (for the case of identical boundary conditions for temperature and salinity). The construction of the general stability chart in the S_1–S_2 plane (independent of wave number β) by transformation from the l_{20}–l_{40} plane is described in Section 4.2. The straight lines HJ and JI in Fig. 3 represent the axes $S_1 = 0$ and $S_2 = 0$. They are obtained from equations (12) and (15) in the form

$$\begin{aligned} S_1 = 0 &\Rightarrow l_{20}\xi_{42}/E_2 = l_{40}\xi_{22}/E_4 + \delta_2\xi_{42} - \delta_4\xi_{22} \\ S_2 = 0 &\Rightarrow l_{20}\xi_{41}/E_2 = l_{40}\xi_{21}/E_4 + \delta_2\xi_{41} - \delta_4\xi_{21}. \end{aligned} \tag{22}$$

Envelope B_d is tangent, by construction, to all the lines B_{2d}, and is also tangent to the four straight lines $l_{20} = 0$, $l_{40} = 0$, $S_1 = 0$, $S_2 = 0$.

4.2. *The stability chart in the Rayleigh number plane* S_1–S_2

Relationships (12) and (15) between l_{20}, l_{40} and S_1, S_2 are used to transform the marginal stability curves from the abstract l_{20}–l_{40} plane to the physical Rayleigh number plane S_1–S_2. The expressions are linear, with coefficients ξ, δ and E which depend on wave number β. Substitution of equations (12) and (15) into equations (13) and using also equations (A6) yield the equations of the static and dynamic marginal stability lines B_{rest} and B_d (in terms of S_1 and S_2)

$$B_{\text{rest}} \rightarrow \begin{cases} \text{(a)} \quad S_1\eta_1 P_2^2(P_1+\gamma_0) - S_2\eta_2 P_1^2(P_2+\gamma_0) \\ \qquad = \gamma(P_1+P_2)(P_1+\gamma_0)(P_2+\gamma_0) \\ \text{(b)} \quad S_1\eta_1 - S_2\eta_2 = \gamma\,;\ \eta_2 S_2 \leqslant \gamma \dfrac{P_1+\gamma_0}{(P_2-P_1)} \end{cases} \tag{23}$$

$$B_{\text{d}} \rightarrow \begin{cases} \text{(a)} \quad S_1\eta_1 P_2^2 = [\sqrt{(S_2\eta_2 P_1^2)} + \sqrt{(\gamma(P_2^2 - P_1^2))}]^2 \\ \text{(b)} \quad S_1\eta_1 - S_2\eta_2 = \gamma\,;\ \eta_2 S_2 \leqslant \gamma \dfrac{P_1^2}{(P_2^2 - P_1^2)} \end{cases} \tag{24}$$

where coefficients η_1, η_2, γ and γ_0, defined in equations (A9), are independent of S_1, S_2, P_1, P_2 and Re. γ and γ_0 depend on the boundary conditions (identical, here, for temperature and salinity), the shape of the trial functions $\phi(z)$ and $\theta(z)$ and wave number β. η_1 and η_2 depend only on ϕ, θ and the initial (undisturbed) distributions $\mathring{T}_j$. B_{d} does not depend on $\mathring{u}$, because it is the envelope of the family of marginal stability lines with Re as a parameter.

We seek now the general stability boundary for any arbitrary perturbation, i.e. the envelope of the family of the marginal stability lines with β as a parameter.

As mentioned above, η_1 and η_2 do not depend on β. Therefore, part (b) of the static stability margin B_{rest}, equations (23), is a straight line with a slope which is not a function of β. The envelope of these lines, B^*_{rest} (b), is the straight line, with the same slope and for a critical value, β^*, of the wave number (Fig. 1(b)). This result has also been obtained by Nield [16].

The second part of B_{rest}, equations (23), moves and rotates when β varies. The envelope of these lines is also shown in Fig. 1(b), and the marginal static stability line, B^*_{rest}, is the combination of these two envelopes, as shown in the figure.

Part B_{d} (b) of the dynamic stability boundary, equations (24), is identical to B_{rest} (b). Part B_{d} (a) is an upper branch of an inclined parabola. As can be seen from equations (23) and (24), the lines B_{d} and B_{rest} (b) depend on β through γ only. Therefore, the limiting positions of these three lines is obtained by substitution of the minimal value of γ, denoted by γ^*, into equations (23) and (24), i.e.

$$B^*_{\text{rest}}\,(\text{b}) = B_{\text{rest}}\,(\text{b})|_{\gamma=\gamma^*}\,; \quad B^*_{\text{d}} = B_{\text{d}}|_{\gamma=\gamma^*}. \tag{25}$$

As γ^* is the minimum function $\gamma(\beta)$, it is found by the condition $\mathrm{d}\gamma/\mathrm{d}\beta = 0$. This relation and equations (A9) lead to the following equation for the critical wave number, β^* (corresponding to γ^*)

$$2\beta^6 + \beta^4\left[\frac{\langle(\mathrm{D}\theta)^2\rangle + h_2\theta^2(1) + h_1\theta^2(0)}{\langle\theta^2\rangle} + \frac{\langle(\mathrm{D}\phi)^2\rangle}{\langle\phi^2\rangle}\right]$$

$$- \frac{\langle(\mathrm{D}\theta)^2\rangle + h_2\theta^2(1) + h_1\theta^2(0)}{\langle\theta^2\rangle} \frac{\langle(\mathrm{D}^2\phi)^2\rangle}{\langle\phi^2\rangle} = 0. \tag{26}$$

This equation has a single real positive root, denoted by β^* and γ^* is given by equations (A9) with $\gamma^* = \gamma(\beta^*)$. The line B^*_{rest} (a) is found from equations (14) using equations (23)

$$B^*_{\text{rest}}\,(\text{a}) = \begin{cases} S_1\eta_1 = \dfrac{P_2+P_1}{P_2-P_1}\left(\dfrac{P_2+\gamma_0}{P_2}\right)^2 \\ \qquad \times \left[\gamma + (P_1+\gamma_0)\dfrac{\gamma'}{\gamma'_0}\right] \\ S_2\eta_2 = \dfrac{P_2+P_1}{P_2-P_1}\left(\dfrac{P_1+\gamma_0}{P_1}\right)^2 \\ \qquad \times \left[\gamma + (P_2+\gamma_0)\dfrac{\gamma'}{\gamma'_0}\right]. \end{cases} \tag{27}$$

This is a parametric representation of the line B^*_{rest} (a) in the plane S_1–S_2 where $\gamma' \equiv \mathrm{d}\gamma(\beta^2)/\mathrm{d}\beta^2$; $\gamma'_0 \equiv \mathrm{d}\gamma_0(\beta^2)/\mathrm{d}\beta^2$. In the same way the line $B^*_{3\text{d}}$ can be found as the envelope of the family of lines $B^*_{3\text{d}}(\beta)$. This operation requires a numerical procedure; however, a good upper bound approximation for the lines B^*_{rest} (a) and $B^*_{3\text{d}}$ can be obtained by substitution of β^* instead of β into equations (23), since the dependence of γ_0 on β is much weaker than that of γ.

A lower bound to the stability boundary B_{d} can also be found. Examination of equations (24) shows that the inclination angle, ψ, of the parabola axis is independent of wave number, β. Also, since the first trial functions do not change their sign, thus by using the mean-value theorem, we obtain

$$\operatorname{tg}\psi = \frac{[\mathrm{D}\mathring{T}_2(z)]_{\text{av}}}{[\mathrm{D}\mathring{T}_1(z)]_{\text{av}}}\left(\frac{P_1}{P_2}\right)^2. \tag{28}$$

This result for the lower bound has also been obtained by Bouscher *et al.* [17].

A general qualitative description of the stability chart in the plane S_1–S_2 is quite impossible, because of the dependence on many physical parameters and boundary conditions. Section 4.1 includes, however, a discussion of the chart in the abstract plane l_{20}–l_{40}, where the results are general and can be applied regardless of the values of these parameters. As mentioned above, a domain in the parametric space is found where the flow is stable for longitudinal disturbances in the flow direction but unstable for general 3-D perturbations, see region S in Fig. 2. The results of this section and Section 4.1 are used to investigate the stability chart in the S_1–S_2 plane for some specific examples.

5. EXAMPLES

The method developed here is demonstrated by its application to two special cases and the comparison of the results with known solutions.

5.1. *Linear initial distributions and ideal boundary conditions*

The temperature and salt concentration are constant on the two boundaries which are free, see equations (4)

$$h_1 = h_2 = \infty; \quad D\hat{T}_1 \equiv D\hat{T}_2 \equiv 1; \quad \hat{u}(z) \equiv 1$$
$$T_1 = T_2 = 0; \quad w = 0; \quad D^2 w = 0 \quad \text{at} \quad z = 0,1. \tag{29}$$

In this case, the operators in equations (3) have constant coefficients and the eigenfunctions of the first mode are $\sin \pi z$. When these are introduced instead of the trial functions, the characteristic equation (8) is exact, and can be written as

$$(\sigma+iR)^3(\pi^2+\beta^2)+(\sigma+iR)^2(\pi^2+\beta^2)^2$$
$$\times(P_1P_2+P_1+P_2)+(\sigma+iR)[(\pi^2+\beta^2)^3(P_1+P_2+1)$$
$$-\beta^2(S_1P_2-S_2P_1)]+(\pi^2+\beta^2)$$
$$\times[(\pi^2+\beta^2)^3-\beta^2(S_1-S_2)] = 0. \tag{30}$$

This equation is of a third order in $(\sigma+iR)$ (and not in σ only) and has real coefficients. Therefore, Re (or R) affects here the character of the instability, i.e. change it from monotonic to oscillatory and vice versa, but cannot affect its onset. A similar result has been obtained by Pnueli and Zvirin [18]. The dynamic marginal stability boundary is identical to the static one, $B_{rest} = B_{3d} = B_d$. Its shape, given by equations (23), coincides with the exact well-known form, e.g. Nield [16]. In this case

$$\gamma/\eta = \frac{(\pi^2+\beta^2)^3}{\beta^2}; \quad \gamma_0 \equiv 1; \tag{31}$$
$$\beta^* = \pi/\sqrt{2} = 2.22144; \quad \gamma^* = 27\pi^4/4 = 657.511.$$

5.2. *Realistic boundary conditions*

Rigid lower and free top boundaries with a parabolic velocity distribution; constant temperature and salinity on both boundaries and linear initial distributions in between. These are written as

$$h_u = h_l = \infty; \quad D\hat{T}_1(z) \equiv D\hat{T}_2(z) \equiv 1$$
$$\hat{u}(z) = \tfrac{3}{2}(2z-z^2) \tag{32}$$
$$T_1 = T_2 = 0; \quad w = 0; \quad Dw = 0 \quad \text{at} \quad z = 0$$
$$T_1 = T_2 = 0; \quad w = 0; \quad D^2 w = 0 \quad \text{at} \quad z = 1.$$

As can be seen by comparison with the previous example, the change of the conditions from free to rigid boundary leads to a much more complicated problem: the coefficients in equations (3) are not constant now, and it is impossible to obtain an exact closed form analytical solution, cf. Chandrasekhar [2]. Let us choose the trial functions as the simplest polynomials satisfying the boundary conditions

$$\theta = z(1-z); \quad \phi = z^2(3-5z+2z^2). \tag{33}$$

Inserting these into equations (A9) and (26) we obtain

$$\gamma = (19\beta^4+432\beta^2+4536)(\beta^2+10)/19\beta^2$$
$$\gamma_0 = \frac{(19\beta^2+216)(\beta^2+10)}{(19\beta^4+432\beta^2+4536)}$$
$$\eta = 507/532; \quad \frac{\partial\gamma}{\partial\beta^2} = 0 \Rightarrow \beta^* = 2.670;$$
$$\gamma^*/\eta = 1140. \tag{34}$$

The ratio γ^*/η represents the critical Rayleigh number for the case of a single gradient: $S_2 = S_{2_{cr}} = \gamma/\eta_2$ for $S_1 = 0$ and $S_1 = S_{1_{cr}} = \gamma/\eta_1$ when $S_2 = 0$, see equations (24). Exact values of $S_{1_{cr}} = 1100.657$ and $\beta^* = 2.68$ have been obtained by Chandrasekhar [2] (for the case of thermal stability without salinity effects). Hence the present method yields a good approximation—within 3% of the exact solution.

It is noted that unlike the previous example, the static and dynamic marginal stability curves here are different. The former is obtained from equations (23) and (34) for various values of wave number, β. The results are listed in Table 1, which also contains accurate values of points on the static stability lines, derived by general Galerkin and continuation methods in ref. [8]. As can be seen, the present first-order approximation yields quite good results; the maximum deviation in Table 1 is 7.2%. The agreement between the results becomes better when β increases and also for large Rayleigh numbers S_1 and S_2.

The dynamic marginal stability lines for various Reynolds numbers, Re, were obtained by the method outlined in Section 4. These lines must be derived numerically and a computer program was developed for it. The results presented here are the envelopes of the marginal stability families of curves with β as a parameter, i.e. the stability boundaries for all possible wave numbers. Figure 4 includes a comparison of the present results with those of the accurate derivation of ref. [8], for $Re = 10^5$. The first approximation underestimates the accurate solution; the deviation between the two lines increases with S_1 and S_2, and its maximum in the range of the figure is 9%.

The stability boundary also includes envelope B_d of the dynamic marginal stability lines for all values of Re. The parabola B_d is obtained from equations (24) and (34).

Figure 5 includes the stability chart in the Rayleigh number plane. In this example $P_1 = 7$, $P_2 = 700$ and $\beta = \beta^* = 2.670$, see equations (34). The static (rest) stability margins are the straight lines GO and ON. The dynamic stability boundaries for the various indicated Reynolds numbers have been obtained by the numerical procedure mentioned above. The envelope, B_d, of these lines is the parabola GLAB shown in Fig. 5.

Figure 6 is an expansion of region NAB of Fig. 5, illustrating the effects of the Reynolds number on the stability nature of the flow. Envelope B_d is the line OB′ in the figure, representing the dynamic stability margin: the region below it is stable for any Re. The static stability line is ON′ (for $Re = 0$), above which every state is unstable. The stability chart in Fig. 6 also includes lines illustrating typical states of solar ponds. Salt water ponds are considered, where the

Table 1. Static oscillatory marginal stability lines: the thermal Rayleigh number, S_1, as a function of the saline Rayleigh number, S_2, for various values of wave number β: FO, present first-order Galerkin method; AC, accurate general Galerkin method [8]

β		S_2										
		10^1	6×10^1	2×10^2	10^3	10^4	10^5	10^6	10^7	10^8	10^9	10^{10}
0.0518	FO					9.77×10^5	9.78×10^5	9.86×10^5	1.07×10^6	1.91×10^6	1.03×10^7	
	AC					9.14×10^5	9.16×10^5	9.25×10^5	1.01×10^6	1.88×10^6	1.05×10^7	
0.139	FO				1.36×10^5	1.36×10^5	1.38×10^5	1.46×10^5	2.30×10^5	1.07×10^6		
	AC				1.27×10^5	1.28×10^5	1.29×10^5	1.37×10^5	2.24×10^5	1.09×10^6		
0.728	FO			1.94×10^4	1.94×10^4	1.95×10^4	2.05×10^4	2.87×10^4	1.13×10^5			
	AC			1.81×10^4	1.82×10^4	1.83×10^4	1.93×10^4	2.78×10^4	1.14×10^5			
1.000	FO		3.16×10^3	3.16×10^3	3.18×10^3	3.25×10^3	4.13×10^3	1.25×10^4				
	AC		2.97×10^3	2.97×10^3	2.99×10^3	3.07×10^3	3.98×10^3	1.25×10^4				
2.682	FO	1.17×10^3	1.17×10^3	1.17×10^3	1.18×10^3	1.26×10^3	2.08×10^3	1.03×10^4				
	AC	1.11×10^3	1.11×10^3	1.12×10^3	1.13×10^3	1.21×10^3	2.04×10^3	1.03×10^4				
7.195	FO		5.04×10^3	5.04×10^3	5.06×10^3	5.13×10^3	5.92×10^3	1.39×10^4	9.32×10^4			
	AC		4.91×10^3	4.92×10^3	4.93×10^3	5.00×10^3	5.80×10^3	1.38×10^4	9.30×10^4			
19.30	FO				1.53×10^5	1.54×10^5	1.54×10^5	1.62×10^5	2.41×10^5	1.03×10^6		
	AC				1.52×10^5	1.53×10^5	1.53×10^5	1.61×10^5	2.40×10^5	1.03×10^6		
51.77	FO						7.36×10^6	7.37×10^6	7.44×10^6	8.23×10^6	1.61×10^7	9.50×10^7
	AC						7.35×10^6	7.36×10^6	7.43×10^6	8.22×10^6	8.22×10^7	9.50×10^7

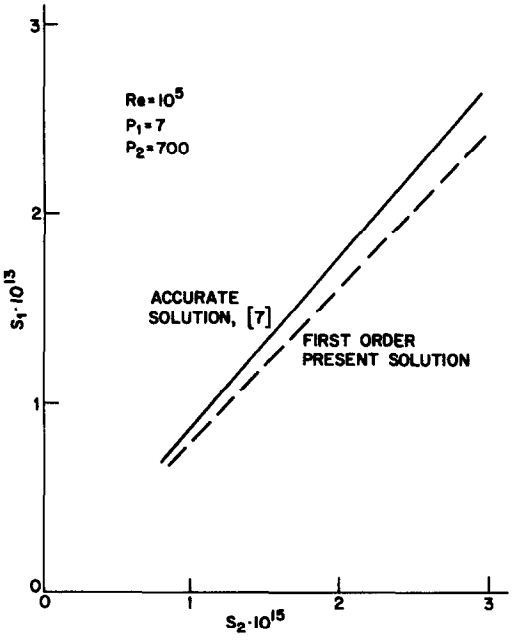

FIG. 4. The dynamic marginal stability line for $Re = 10^5$ (comparison of the present first-order approximation and the accurate results of ref. [7]).

temperature difference is taken as $\Delta T_1 = 60°C$. Obviously, ΔT_1 should be the highest possible for maximum efficiency. It is well known that a bottom layer temperature of about 95°C can be reached. The lines in Fig. 6 represent ponds of various depths for two values of the salinity difference (100 and 300 kg m^{-3}). These lines are linear, because the ratio S_1/S_2 does not depend on d.

As can be seen from the figure, when the depth, d, increases, the critical Reynolds number increases too. In the range of d between 0.8 and 2 m, doubling the depth causes an increase of Re_{cr} by a factor of about 3. Thus, if the same velocity is kept in the pond while the depth is increased, there is no danger of destabilizing the flow. Depth values below, say, 1 m, should be avoided because the pond would be too close to the marginal stability line.

6. DISCUSSION

This paper describes a technique for the construction of the static and dynamic stability chart of double diffusive shear flows, based on a first approximation Galerkin method.

As mentioned above, this relatively simple method is not generally accurate. Its limitations and advantages are discussed here and an outline is suggested for the proper utilization of the procedure and results.

It should be emphasized that a first-order Galerkin method may lead, in some cases, to results which are not only inaccurate but utterly wrong. For example, the first-order approximation predicts that plane Poiseuille flow is always stable, while it is known, based on higher order analyses, that instabilities do exist, cf. refs. [6, 10]. Thus great care must be taken when a first-order Galerkin technique is attempted. The method can be used effectively for certain purposes and under several conditions; it is recommended, however, to support the results by other, more accurate, means as explained below.

The first approximation Galerkin method is shown below to be useful for the following main applications.

(a) First approximation, as a preparation for more accurate calculations.

(b) Parametric study of the stability behaviour of the flow, when it yields reasonably accurate results.

(c) Derivation and evaluation of the general qualitative form of the stability chart.

As pointed out in refs. [6, 7, 10], the accurate solution by a general Galerkin method involves high-order complex matrices for cases of non-self-adjoint operators with complex variable coefficients. Thus the numerical determination of the eigenvalues is con-

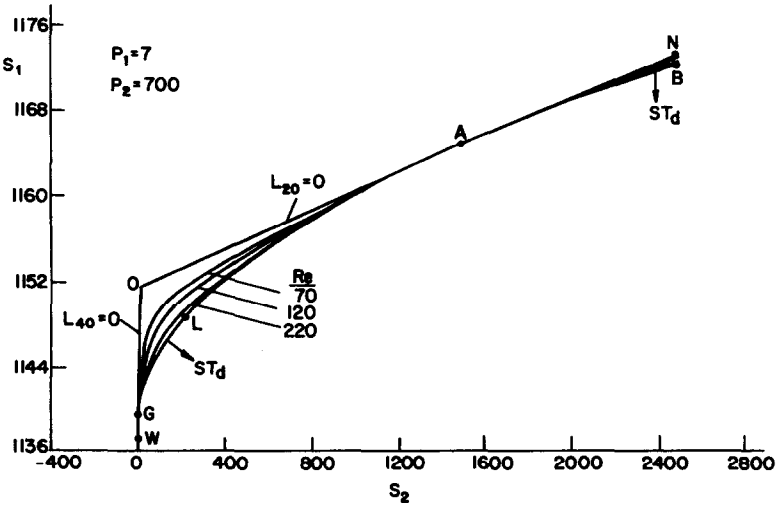

FIG. 5. Marginal stability boundaries for various values of Re in the Rayleigh number plane, obtained by a first approximation Galerkin method.

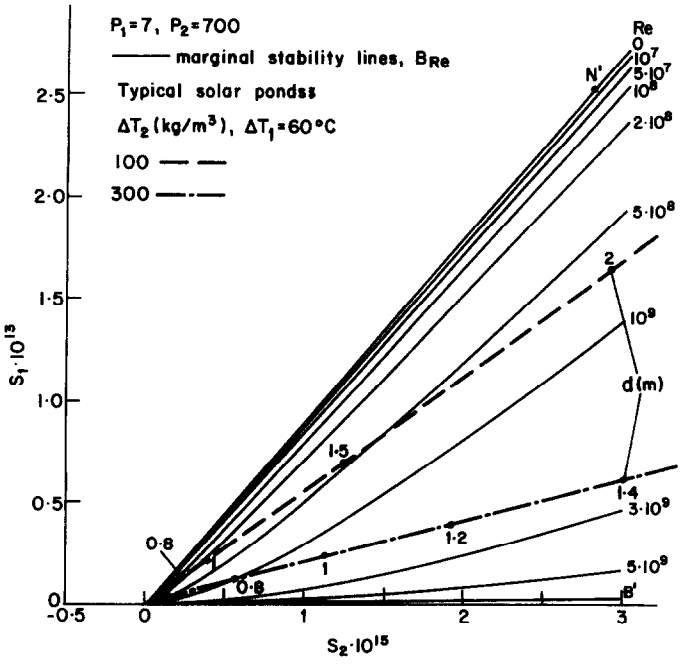

FIG. 6. The stability chart in the Rayleigh number plane (expansion of region NAB in Fig. 5), including lines representing states of typical solar ponds.

sidered a difficult task. Moreover, problems such as 'spurious' eigenvalues may be encountered. On the other hand, for the derivation of the stability chart, only one eigenvalue is actually required—that with the largest real part. The approach developed in ref. [8] simplifies the analysis by using a combination of the methods of 'vector iteration with shift' and 'continuation'. The effectiveness of this approach strongly depends on the initial guess for the marginal stability curves. The first approximation method described above provides, indeed, a good initial guess. It is further noted that this method is analytical and does not require numerical computations to obtain the eigenvalues. The marginal stability lines have been derived directly from the coefficients of the characteristic stability equation. The calculations of the eigenvalues in ref. [8] have been performed very carefully in order to isolate a single one with the largest real part and determine it accurately on a marginal stability line. The continuation method enables, then, progressive 'drawing' of the line by investigating the variation of the eigenvalue with respect to the system parameters.

Even the simplified and efficient method of ref. [8] to derive the stability chart by a general Galerkin method is still quite complicated and expensive, i.e. it requires significant computer time and memory. Therefore, if a reasonably accurate derivation by a first approximation is available, such as the method presented here, a parametric study and an investigation of various phenomena and effects can be performed much more conveniently. It is reminded, again, that the accuracy of the first approximation must be examined by spot-checking (at least).

It has been shown here and in ref. [9] that for certain cases of boundary conditions the method yields the exact solutions, because the trial functions are the exact eigenfunctions of equations (3). Furthermore, if the operator of these equations is self-adjoint, there exists, then, a variational principle for the problem. The Galerkin procedure is identical to the Rayleigh–Ritz method, and the extremum properties of the eigenvalues can be utilized. For more complicated cases such as the realistic boundary conditions, the present method sometimes yields good approximations, as has been shown by a comparison with the accurate derivation of ref. [8]. It can be deduced that the present method would lead to good approximations when the parameters appearing in equations (3) are in the neighborhood of those leading to self-adjoint operators, and when the Reynolds number is small and the initial temperature and salinity distributions are close to linear.

The third application of the proposed method is the qualitative derivation and evaluation of the general properties of the stability chart. As pointed out above, an accurate derivation is quite complicated and expensive. The chart consists, generally, of various regions and numerous marginal lines of static and dynamic stability. Without preliminary information of at least several main regions of the chart, it would be extremely difficult to know what lines and zones to search and where (approximately) to start the procedure of finding them. The first-order Galerkin method developed here provides the tool for such an initial general outline of the stability chart.

An example for a peculiar stability phenomenon is the result of a flow which is stable for 2-D disturbances in the flow direction (transverse rolls) and per-

pendicular to it (longitudinal rolls), but unstable for certain oblique 3-D perturbations. A similar result has been obtained by ref. [12] for plane Poiseuille flow. This phenomenon is explained by the non-monotonic effect of the viscosity, and leads to the behaviour of two marginal stability lines (for 2-D disturbances) crossing at certain points in the chart. One of these lines is obviously a 'dummy'.

Another example is plane Quette flow, or semi-parabolic plane Poiseuille flow (rigid–free boundaries), which are linearly stable for all Reynolds numbers, Re, and wave number, β. This situation corresponds to the origin, $S_1 = S_2 = 0$, of the Rayleigh number plane. Thus there exists a region surrounding this point where the shear stratified flow is also stable for all Re and β.

7. CONCLUSIONS

A first-order Galerkin method has been developed for the stability study of double diffusive shear flows. The method can be used, in general, for a qualitative derivation and evaluation of the stability chart and as an initial guess for a more accurate solution. Comparison to previous results obtained by a general Galerkin technique has shown that the approximation obtained by the present method is reasonable; it was therefore used for a detailed analysis of the stability chart.

The stability chart in the Rayleigh number plane S_1–S_2 was derived in this plane for various Reynolds numbers, including the rest state ($Re = 0$). The stability regions for various Reynolds numbers, ST_{Re}, and for all Re, ST_d, have been obtained as well as the line dividing between them, B_d, which is the envelope of the crossing lines B_{Re}. This envelope is tangent to the monotonic and oscillatory static stability boundaries, to axes S_1 and S_2 and to all the lines B_{Re}.

A domain in the parametric space has been discovered, where the flow is stable for 2-D transverse and longitudinal rolls, but unstable with respect to general 3-D disturbances.

REFERENCES

1. S. Ostrach, Convection in fluids heated from below, *Trans. ASME* **79,** 299–305 (1975).
2. S. Chandrasekhar, *Hydrodynamic and Hydromagnetic Stability*. Oxford University Press, Oxford (1961).
3. Z. H. Qureshi and B. Gebhart, The stability of vertical thermal buoyancy induced flows in cold pure and saline water, *Int. J. Heat Mass Transfer* **29,** 1383–1392 (1986).
4. G. Veronis, Effect of a stabilizing gradient of solute on thermal convection, *J. Fluid Mech.* **34,** 315–336 (1968).
5. D. Pnueli and S. Iscovici, Sufficient conditions for stability of completely confined fluids, *Israel J. Technol.* **8,** 209–215 (1970).
6. S. A. Orszag, Accurate solution of the Orr–Sommerfeld stability equation, *J. Fluid Mech.* **50,** 689–703 (1971).
7. M. Magen, D. Pnueli and Y. Zvirin, The stability chart of parallel shear flows with double diffusive processes—general properties, *J. Engng Math.* **19,** 175–187 (1985).
8. M. Magen, D. Pnueli and Y. Zvirin, The stability chart of double diffusive processes with shear flow—construction by the Galerkin and continuation methods, *J. Engng Math.* **20,** 127–144 (1986).
9. D. A. Nield, The onset of transient convective instabilities, *J. Fluid Mech.* **71,** 441–454 (1975).
10. C. E. Grosch and H. Salwen, The stability of steady and time-dependent plane Poiseuille flow, *J. Fluid Mech.* **34,** 177–205 (1968).
11. H. B. Squire, On the stability for three-dimensional disturbances of viscous flow between parallel walls, *Proc. R. Soc.* **A142,** 621–628 (1933).
12. M. Magen and A. T. Patera, Three-dimensional linear instability of parallel shear flows, *Physics Fluids* **29,** 364–367 (1986).
13. S. G. Mikhlin, *Direct Methods in Mathematical Physics* (in Russian). Gos. Izd. Technico-Teor. Lit., Moskwa-Leningrad (1950).
14. F. R. Gantamakher, *Matrix Theory*. Chelsea, New York (1959).
15. M. Magen, Thermohaline stability with general horizontal flows, D.Sc. thesis, Technion, Haifa, Israel (1983).
16. D. A. Nield, The thermohaline Rayleigh–Jeffreys problem, *J. Fluid Mech.* **29,** 545–558 (1967).
17. M. Bouscher, D. Pnueli and Y. Zvirin, Rayleigh–Jeffreys stability of thermohaline stratified fluids subject to arbitrary gradients, *Desalination* **49,** 17–36 (1984).
18. D. Pnueli and Y. Zvirin, Rayleigh–Jeffreys stability of thermohaline stratified fluids subject to horizontal flows, *Desalination* **33,** 163–183 (1980).

APPENDIX: THE COEFFICIENTS AND PARAMETERS IN THE CHARACTERISTIC EQUATION (8) AND THE STABILITY CRITERIA

The (3×3) matrices N and M in equation (7) are obtained after several integrations by parts as

$$
\begin{aligned}
N_{jj} &= -[\langle (\mathrm{D}\theta_j)^2 + \beta^2\theta_j^2\rangle + h_{u_j}\theta_j^2(1) + h_{l_j}\theta_j^2(0)] - \mathrm{i}RP_j\langle \mathring{u}\theta_j^2\rangle \\
N_{33} &= -\langle (\mathrm{D}^2\phi)^2 + 2\beta^2(\mathrm{D}\phi)^2 + \beta^4\phi^2\rangle - \mathrm{i}R\left\langle \mathring{u}[(\mathrm{D}\phi)^2 + \beta^2\phi^2] + \frac{\phi^2}{2}\mathrm{D}^2\mathring{u}\right\rangle \qquad \text{(A1)} \\
N_{12} &= N_{21} = 0; \quad N_{j3} = \langle \phi\theta_j D\mathring{T}_j\rangle; \quad N_{3j} = (-1)^{j+1}\beta^2 S_j\langle \theta_j\phi\rangle \\
M_{jj} &= P_j\langle \theta_j^2\rangle; \quad M_{33} = \langle (\mathrm{D}\phi)^2 + \beta^2\phi^2\rangle; \quad M_{kj} = M_{kk}\delta_{kj} \quad k = 1,2,3; j = 1,2
\end{aligned}
$$

where

$$\langle \ldots \rangle \equiv \int_0^1 \ldots \mathrm{d}z.$$

The coefficients a_j of the characteristic equation (8) are given by

$$\begin{aligned} a_1 &= -\left(\frac{N_{11}}{M_{11}}+\frac{N_{22}}{M_{22}}+\frac{N_{33}}{M_{33}}\right) \\ a_2 &= \frac{N_{11}N_{22}}{M_{11}M_{22}}+\frac{N_{22}N_{33}}{M_{22}M_{33}}+\frac{N_{33}N_{11}}{M_{33}M_{11}}-\frac{N_{23}N_{32}}{M_{22}M_{33}}-\frac{N_{13}N_{31}}{M_{11}M_{33}} \\ a_3 &= -\frac{N_{11}N_{22}N_{33}}{M_{11}M_{22}M_{33}}+\frac{N_{11}}{M_{11}}\frac{N_{23}N_{32}}{M_{22}M_{33}}+\frac{N_{22}}{M_{22}}\frac{N_{13}N_{31}}{M_{11}M_{33}}. \end{aligned} \tag{A2}$$

In order to construct the marginal stability lines, parameters b_k, c_k and L_i, which appear in equations (9) and (10), must be expressed as functions of the elements of matrices N and M. For this we define

$$\begin{aligned} &B_k \equiv -\mathrm{Re}\,(N_{kk})/M_{kk}\,; \quad RD_k \equiv -\mathrm{Im}\,(N_{kk})/M_{kk} \\ &S_jA_j \equiv (-1)^{j+1}N_{3j}N_{j3}/M_{jj}M_{33}\,; \quad k=1,2,3\,; \quad j=1,2 \end{aligned} \tag{A3}$$

and from equations (A3), (A2) and (A1)

$$\begin{aligned} b_1 &= B_1+B_2+B_3, \quad c_1 = R(D_1+D_2+D_3) \\ b_2 &= B_1B_2+B_2B_3+B_3B_1-R^2(D_1D_2+D_2D_3+D_3D_1)-S_1A_1+S_2A_2 \\ c_2 &= R[B_1(D_2+D_3)+B_2(D_3+D_1)+B_3(D_1+D_2)] \\ b_3 &= B_1B_2B_3-R^2(B_1D_2D_3+B_2D_3D_1+B_3D_1D_2)-S_1A_1B_2+S_2A_2B_1 \\ c_3 &= R(B_1B_2D_3+B_2B_3D_1+B_3B_1D_2-R^2D_1D_2D_3-S_1A_1D_2+S_2A_2D_1). \end{aligned} \tag{A4}$$

Finally, parameters L_j are obtained from equations (A4) and (10) as

$$\begin{aligned} L_1 &= B_1+B_2+B_3\,; \quad L_2 = b_1[(B_1+B_2)(B_2+B_3)(B_3+B_1) \\ &\quad -A_1S_1(B_3+B_1)+A_2S_2(B_3+B_2)]+R^2[B_1B_2(D_1-D_2)^2 \\ &\quad +B_2B_3(D_2-D_3)^2+B_3B_1(D_3-D_1)^2] \\ L_3 &= L_2^2L_4-(2b_1L_5+c_2L_2)^2 \\ L_4 &= 4b_1[B_1B_2B_3-A_1S_1B_2+A_2S_2B_1]+R^2[B_1^2(D_2-D_3)^2 \\ &\quad +B_2^2(D_3-D_1)^2+B_3^2(D_1-D_2)^2-2B_1B_2(D_2-D_3)(D_3-D_1) \\ &\quad -2B_2B_3(D_3-D_1)(D_1-D_2)-2B_3B_1(D_1-D_2)(D_2-D_3)] \\ L_5 &= -R\{D_1B_2B_3[b_1^2-B_1^2+R^2(D_2-D_3)^2]+D_2B_3B_1[b_1^2-B_2^2 \\ &\quad +R^2(D_3-D_1)^2]+D_3B_1B_2[b_1^2-B_3^2+R^2(D_1-D_2)^2]-S_1A_1[D_2(b_1^2-B_2^2) \\ &\quad -B_2(D_1B_1+D_3B_3)]+S_2A_2[D_1(b_1^2-B_1^2)-B_1(D_2B_2+D_3B_3)]\}. \end{aligned} \tag{A5}$$

For the static case, with no initial flow in the undisturbed state, ($R=0$), the parameters L_2 and L_4 are given by equations (12), with coefficients

$$\left.\begin{aligned} &\delta_2(\beta) \equiv b_1(B_1+B_2)(B_2+B_3)(B_3+B_1)\,; \quad \delta_4(\beta) = 4b_1B_1B_2B_3 \\ &\xi_{21}(\beta) = b_1A_1(B_3+B_1)\,; \quad \xi_{22}(\beta) = b_1A_2(B_3+B_2) \\ &\xi_{41}(\beta) = 4b_1A_1B_2\,; \quad \xi_{42}(\beta) = 4b_1A_2B_1. \end{aligned}\right\} \tag{A6}$$

Coefficients $E(\beta)$ which appear in equations (15) are obtained in the following manner. For identical temperature and salinity boundary conditions $h_{u_1}=h_{u_2}=h_u$, $h_{l_1}=h_{l_2}=h_l$ (see equations (4)). Introducing these relations together with the choice of $\theta_1(z)=\theta_2(z)=\theta(z)$ into equations (A1) and (A3), one obtains

$$\left.\begin{aligned} D_1 &= D_2 = \langle \hat{u}(z)\theta^2(z)\rangle/\langle\theta^2(z)\rangle \\ D_3 &= \langle \hat{u}[(\mathrm{D}\phi)^2+\beta^2\phi^2]+0.5\phi^2\mathrm{D}^2\hat{u}\rangle/\langle(\mathrm{D}\phi)^2+\beta^2\phi^2\rangle. \end{aligned}\right\} \tag{A7}$$

Substitution of equations (A7) into equations (A5) yields, after some manipulations, the following expressions of coefficients $E(\beta)$ of equations (15) (see also equations (A4)) and the last of equations (15)

$$\left.\begin{aligned} E_2 &= 2b_1^3\frac{B_1B_2}{B_1+B_2}\,; & E_4 &= 4b_1^3\frac{B_1B_2}{B_3} \\ E_3 &= 16\frac{b_1^9B_1^3B_2^3}{B_3(B_1+B_3)^2}\,; & E_r &= \frac{4b_1^3B_1B_2}{(D_1-D_3)^2B_3(B_1+B_2)}. \end{aligned}\right\} \tag{A8}$$

Coefficients η_1, η_2, γ and γ_0 in equations (23) and (24) for the static stability boundaries in the plane S_1–S_2 are obtained

by introduction of equations (12) and (15) into equations (13)

$$\left.\begin{aligned}\gamma &= \frac{\langle\beta^4\phi^2+2\beta^2(\mathrm{D}\phi)^2+(\mathrm{D}^2\phi)^2\rangle[\langle\beta^2\theta^2+(\mathrm{D}\theta)^2\rangle+h_u\theta^2(1)+h_l\theta^2(0)]}{\beta^2\langle\phi^2\rangle\langle\theta^2\rangle}\\ \gamma_0 &= \frac{[\langle\beta^2\theta^2+(\mathrm{D}\theta)^2\rangle+h_u\theta^2(1)+h_l\theta^2(0)]}{\langle\theta^2\rangle}\,\frac{\langle\beta^2\phi^2+(\mathrm{D}\phi)^2\rangle}{\langle\beta^4\phi^2+2\beta^2(\mathrm{D}\phi)^2+(\mathrm{D}^2\phi)^2\rangle}\\ \eta_j &= \langle\mathrm{D}\hat{T}_j\theta\phi\rangle\langle\theta\phi\rangle/\langle\theta^2\rangle\langle\phi^2\rangle;\ j=1,2.\end{aligned}\right\} \tag{A9}$$

Note that γ and γ_0 depend on β but η_j does not.

DIAGRAMME DE STABILITE DES ECOULEMENTS PARALLELES CISAILLANTS AVEC MECANISMES DOUBLEMENT DIFFUSIFS—OBTENTION APPROCHEE PAR UNE METHODE DE GALERKIN DE PREMIER ORDRE

Résumé— La stabilité d'une couche de fluide soumise à un écoulement cisaillant horizontal quelconque est étudiée dans le cas de distributions verticales arbitraires de température et de salinité. L'analyse de stabilité linéaire est utilisée pour étudier la stabilité sous l'effet de perturbations tridimensionnelles. On utilise une méthode de Galerkin pour dériver l'équation caractéristique ; les conditions de stabilité sont obtenues ainsi que les courbes de stabilité marginales. La méthode est appliquée dans le cas d'une distribution parabolique de vitesse et des profils linéaires de température et de salinité. Le diagramme de stabilité dans le plan des nombres de Rayleigh contient différentes régions stables et instables qui dépendent du nombre de Reynolds. Les résultats sont comparés avec des résultats antérieurs obtenus par une méthode générale de Galerkin. On trouve une région où l'écoulement est stable vis-à-vis de perturbations transversales bidimensionnelles, mais instable pour des perturbations générales tridimensionnelles.

DIE STABILITÄTSKARTE PARALLELER SCHERSTRÖMUNGEN BEI DOPPELDIFFUSIVEN PROZESSEN—NÄHERUNGSWEISE HERLEITUNG MIT EINER GALERKIN-METHODE 1. ORDNUNG

Zusammenfassung—Es wird die Stabilität einer unendlich ausgedehnten Flüssigkeitsschicht, die einer beliebigen horizontalen Scherströmung und einer beliebigen vertikalen Temperatur- und Salzgehaltsverteilung unterworfen ist, betrachtet. Die lineare Stabilitätsanalyse wird verwendet, um die Stabilität unter dem Einfluß allgemeiner dreidimensionaler Störungen zu untersuchen. Um die charakteristischen Gleichungen herzuleiten, wird ein Näherungsverfahren erster Ordnung nach Galerkin verwendet. Man erhält dann die Stabilitätskriterien, und die Rand-Stabilitätskurven können ermittelt werden. Die Methode wird an einem Beispiel mit parabolischer Geschwindigkeitsverteilung und linearer Verteilung der Temperatur und des Salzgehalts angewandt. Es wurde herausgefunden, daß die Stabilitätskurve in der Rayleigh-Zahlen-Ebene abhängig von der Reynolds-Zahl unterschiedlich stabile und instabile Regionen beinhaltet. Die hier ermittelten Ergebnisse werden mit früheren Ergebnissen verglichen, welche mit einer allgemeinen Galerkin-Methode erhalten wurden. Es wurde ein Gebiet gefunden, in dem die Strömung für zweidimensionale transversale Störungen stabil ist, jedoch instabil in Bezug auf allgemeine dreidimensionale Störungen.

ДИАГРАММА УСТОЙЧИВОСТИ ПАРАЛЛЕЛЬНЫХ СДВИГОВЫХ ТЕЧЕНИЙ С УЧЕТОМ ВЗАИМНОЙ ДИФФУЗИИ: ПРИБЛИЖЕННЫЙ РАСЧЕТ МЕТОДОМ ГАЛЕРКИНА ПЕРВОГО ПОРЯДКА

Аннотация—Рассматривается устойчивость бесконечного слоя жидкости при произвольном горизонтальном сдвиговом течении и произвольных вертикальных распределениях температуры и солесодержания. В общем случае трехмерных возмущений устойчивость исследуется в рамках линейной модели. Метод Галеркина первого порядка использован для получения характеристического уравнения, затем установлены условия устойчивости и область ее существования. Применение метода Галеркина рассмотрено на примере с параболическим распределением скорости и линейными распределениями температуры и солесодержания. Диаграмма устойчивости в плоскости чисел Рэлея включает различные устойчивые и неустойчивые области, определяемые числом Рейнольдса. Результаты настоящей работы сравниваются с данными, полученными ранее общим методом Галеркина. Найдена область, в которой поток устойчив в случае поперечных возмущений, но неустойчив к трехмерным возмущениям.